Defect kinetics in spinels: Long-time simulations of $MgAl_2O_4$, $MgGa_2O_4$, and $MgIn_2O_4$

B. P. Uberuaga,[1] D. Bacorisen,[2] Roger Smith,[2] J. A. Ball,[3] R. W. Grimes,[3] A. F. Voter,[1] and K. E. Sickafus[1]
[1]*Los Alamos National Laboratory, Los Alamos, New Mexico 87545, USA*
[2]*Department of Mathematical Sciences, Loughborough University, Loughborough, Leicestershire LE11 3TU, United Kingdom*
[3]*Department of Materials, Imperial College, Prince Consort Road, London SW7 2BP, United Kingdom*
(Received 7 November 2006; revised manuscript received 1 February 2007; published 27 March 2007)

Building upon work in which we examined defect production and stability in spinels, we now turn to defect kinetics. Using temperature accelerated dynamics (TAD), we characterize the kinetics of defects in three spinel oxides: magnesium aluminate $MgAl_2O_4$, magnesium gallate $MgGa_2O_4$, and magnesium indate $MgIn_2O_4$. These materials have varying tendencies to disorder on the cation sublattices. In order to understand chemical composition effects, we first examine defect kinetics in perfectly ordered, or normal, spinels, focusing on point defects on each sublattice. We then examine the role that cation disorder has on defect mobility. Using TAD, we find that disorder creates local environments which strongly trap point defects, effectively reducing their mobility. We explore the consequences of this trapping via kinetic Monte Carlo (KMC) simulations on the oxygen vacancy (V_O) in $MgGa_2O_4$, finding that V_O mobility is directly related to the degree of inversion in the system.

DOI: 10.1103/PhysRevB.75.104116 PACS number(s): 61.43.Bn, 61.82.Ms, 66.30.Lw, 66.30.Hs

I. INTRODUCTION

Ceramic materials are of great interest for a number of nuclear applications, both for fission and fusion reactors. Spinels, in particular, have been proposed as inert matrices for nuclear fuels[1,2] and as radio-frequency windows for fusion reactors.[3–5] In such environments, materials will be subjected to constant irradiation and their resistance to that bombardment is key to their performance. $MgAl_2O_4$ spinel has been shown to be remarkably resistant to radiation damage from neutrons and light ions, exhibiting very little swelling even to high doses,[6,7] though it does exhibit a transition to a rock-salt structure under certain conditions.[8] Spinel is known to amorphize when subjected to fission product or heavy ion irradiation[9,10] or irradiation at very low temperatures.[11]

A material's ability to withstand radiation damage is primarily due to two factors: how much damage is generated during irradiation and how that damage then evolves. Previous work[12–14] has examined the first issue, namely the number and types of defects produced in collision cascades in various Mg-based spinels. That work looked at how disorder, which varies naturally through the series $MgAl_2O_4$, $MgGa_2O_4$, and $MgIn_2O_4$, affects damage production. The second factor, damage evolution, involves both defect recombination as well as aggregation that might lead to amorphization or swelling in some materials. In this paper, we examine point defect mobility in spinel as a function of disorder. The kinetics of point defects will determine how quickly defect recombination can occur. Combined with knowledge of defect stability, defect kinetics will also give insight into probable aggregation mechanisms that eventually lead to, for instance, interstitial loop formation and growth.

In this work, we perform accelerated molecular dynamics[15] and kinetic Monte Carlo[16] simulations on defects in spinels (AB_2O_4) in order to understand the impact that disorder plays on point defect mobility. We simulated three different spinels: normal magnesium aluminate ($MgAl_2O_4$), half-inverse or disordered magnesium gallate ($MgGa_2O_4$), and fully inverse magnesium indate ($MgIn_2O_4$). The amount of inversion i measured as the fraction of B cations that reside on A lattice sites goes roughly from $i \sim 0$ for $MgAl_2O_4$ to $i=0.5-0.6$ for $MgGa_2O_4$ to $i \sim 1$ for $MgIn_2O_4$. The goal of this work is to understand how defect kinetics depends on i.

The structure of part of the normal ($i=0$) spinel unit cell is shown in Fig. 1. Mg^{2+} and Al^{3+} ions occupy fourfold A sites and sixfold coordinated B sites, respectively. The O^{2-} ions have one Mg^{2+} and three Al^{3+} ions as nearest neighbors. Using Wyckoff notation, the positions of the ions with respect to the origin on an A-site cation can be described as A at 8a, B at 16d, and O at 32e (for a normal spinel with no cation disorder). There are interstices (unoccupied symmetry sites) located at 16c (octahedral site) and 8b and 48f (tetrahedral sites).[17] The oxygen ions do not quite occupy perfect cubic positions (as in Fig. 1) but are displaced slightly in ⟨111⟩ directions towards their three octahedral Al^{3+} neighbors. This will be important when examining defect mobility.

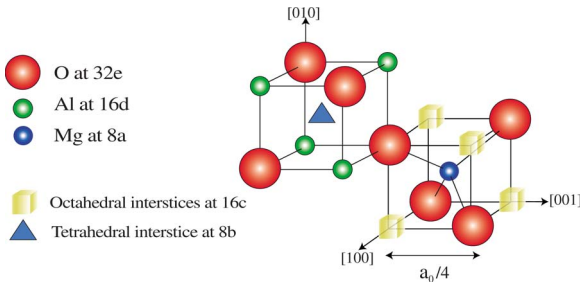

FIG. 1. (Color online) Diagram showing part of the unit cell of normal magnesium aluminate spinel with lattice parameter a_0. Large (red) spheres indicate oxygen, small light (green) spheres are aluminum, and small dark (blue) spheres are magnesium. Cubes indicate interstices at 16c sites and the triangle indicates the interstice at 8b. This scheme will be used to identify atoms in subsequent figures.

II. METHODOLOGY

A. Potential

The calculations were based on a fixed charge model with a pairwise potential energy function $\phi(r_{ij})$ comprised of the standard Buckingham potential and the usual electrostatics potential $V(r_{ij})$ as shown by Eq. (1):

$$\phi(r_{ij}) = A_{ij}\exp\left(-\frac{r_{ij}}{\rho_{ij}}\right) - \frac{C_{ij}}{r_{ij}^6} + V(r_{ij}). \quad (1)$$

Here r_{ij} refers to the distance between the interacting ions i and j. Details for the potential parameters A_{ij}, ρ_{ij}, and C_{ij} are provided in Ref. 13. For the disordered spinels, $2\times1\times1$ unit cells containing 112 atoms and $2\times2\times2$ unit cells containing 448 atoms, representative of the appropriate inversion, were generated by a combined Monte Carlo and energy minimization technique, as described in Ref. 18. The standard Ewald sum was used to calculate the electrostatic part of the potential.

B. Temperature accelerated dynamics

In order to probe the long-time behavior of defects in spinels, we used temperature accelerated dynamics (TAD),[19] one of a number of accelerated molecular dynamics methods.[15] The TAD algorithm has been described extensively elsewhere (see, in particular, Ref. 15). Here we give a brief overview of the method.

TAD involves running molecular dynamics (MD) at a high temperature T_{high} significantly higher than the temperature of interest T_{low}. This MD is constrained such that the trajectory is not allowed to leave the current energy basin of the system. Whenever an event is detected, the event is characterized by finding its saddle point [using the nudged elastic band method (NEB)[20]] and the trajectory is returned to the current basin. The high-temperature MD is then continued. Using the saddle point energy, and assuming harmonic transition state theory, the times of events seen at T_{high} can be extrapolated to T_{low}. Once a stopping criterion is met, depending on an assumed minimum prefactor for the system (here we use $\nu_{\text{min}}=10^{12}$/s) and an uncertainty that the correct event is missed ($\delta=0.05$), the high-temperature MD is stopped, the event with the shortest time at T_{low} is accepted, the trajectory put into the corresponding basin, and the procedure repeated for the new state.

A key component of the TAD procedure is identifying transitions. Here, a transition is said to occur any time that, upon minimization, an atom has moved more than 0.3 Å from its position in the current minimum. In the simulations reported here, T_{low} was typically set to 300 K, though higher values were used in some instances where defect mobility was particularly slow. For T_{high}, we used values between 800 and 3000 K, again depending on the rate at which events occurred. The values given above for δ and ν_{min} are fairly aggressive. However, we typically simulated enough time that we are confident that we did not miss any key events describing the diffusion of the defects considered here. We used simulation cell sizes of 448 atoms with periodic boundary conditions.

C. Kinetic Monte Carlo

In order to understand the impact of inversion on defect diffusion, we performed kinetic Monte Carlo[16] (KMC) simulations on oxygen vacancies in $MgGa_2O_4$ with varying degrees of inversion. Again, the inversion was generated via a combined Monte Carlo/energy minimization procedure.[18] Snapshots of the structure with inversions of $i=0$, 0.05, 0.23, and 0.58 were examined. To perform a KMC simulation, one must know the rates for all possible events to occur. Within harmonic transition state theory, these rates are given by

$$k_j = \nu_j e^{-E_j/k_BT}, \quad (2)$$

where k_j is the rate of event j, ν_j is the frequency prefactor for the event, E_j is the saddle point energy for the event, k_B is the Boltzmann constant, and T is the temperature. For each value of inversion, the barrier for every possible oxygen vacancy migration pathway involving a single moving atom was calculated using NEB. For a cell containing 448 atoms, this resulted in 1536 unique saddle points. These saddle points were then input into a KMC model in which all prefactors were set to the standard value of 10^{13}/s. From the KMC simulations, the diffusion coefficient for a single oxygen vacancy was calculated as a function of temperature and inversion.

We focused in the KMC simulations on the oxygen vacancy just because vacancies are simpler to characterize than interstitials. There is typically only one type of vacancy structure for a given lattice site, while, as the oxygen interstitial in spinels exhibits a split structure,[14,21] there are at least three types of interstitial structures per site. (Though, for high levels of inversion, split vacancy structures do occur. In the KMC simulations, we ignored these states for simplicity.) Similar simulations could be performed for the cation vacancies. However, while the details will differ, we expect the qualitative behavior to be similar to that of oxygen vacancies.

III. KINETICS OF POINT DEFECTS IN NORMAL SPINELS

While none of the spinels considered here occur perfectly ordered in nature, we have begun by performing TAD simulations to characterize point defect mobility in normal or ordered versions of each spinel (i.e., $i=0$). We have done this in order to understand the chemical effects that influence diffusion in these materials, as opposed to the effects of cation disorder, which we will consider in the next section.

A. Normal spinel $MgAl_2O_4$

Table I shows the activation energies and the corresponding mechanisms for point defects to diffuse in normal spinel for the three different compositions. Here, we describe the behavior in $MgAl_2O_4$. Then we will compare and contrast with diffusion in normal $MgGa_2O_4$ and $MgIn_2O_4$.

1. Interstitials

In $MgAl_2O_4$ the oxygen split interstitial defect O_i''-$V_O^{\cdot\cdot}$-O_i'' has the lowest activation energy (0.29 eV) for point defect

TABLE I. Migration activation energies (E_m) for point defect diffusion in normal spinels. All energies are in eV.

	$MgAl_2O_4$		$MgGa_2O_4$		$MgIn_2O_4$	
Defect	E_m	Nature	E_m	Nature	E_m	Nature
O_i''	0.29	1D	0.47	1D	0.54	3D
	0.64, 0.67	rotation	0.79	rotation		
$Mg_i^{\cdot\cdot}$	0.56	3D	0.48	3D	0.32	3D
B_i'''	Not stable for any material; decays to $B_{Mg}^{\cdot}+Mg_i^{\cdot\cdot}$					
$V_O^{\cdot\cdot}$	1.67	3D	2.02	3D	1.83	3D
V_{Mg}''	0.68	3D	0.67	3D	0.97	3D
V_B'''	2.00	3D	1.82	3D	0.90	3D

diffusion, where we have used Kröger-Vink notation to identify defect charges.[22] Its diffusion is one-dimensional in a ⟨110⟩ direction, occurring via an interstitialcy mechanism as illustrated in Figs. 2(a) and 2(b). This mechanism allows the oxygen interstitial to diffuse very quickly, but that diffusion is constrained along a ⟨110⟩ direction. In order to access other ⟨110⟩ directions, the oxygen interstitial can rotate via two mechanisms. These are illustrated in Figs. 2(b)–2(e). These mechanisms have nearly identical barriers of 0.67 and 0.64 eV.

The complex nature of oxygen interstitial diffusion has consequences for interstitial-vacancy recombination. If a vacancy lies along the ⟨110⟩ direction of the interstitial, the interstitial will be strongly attracted to it and quickly recombine. In fact, this is seen in collision cascades.[14] However, if the two defects are not aligned, the oxygen interstitial is still attracted to the vacancy and diffuses towards the vacancy such that it minimizes the distance between the two defects given the constraint that it has to remain on the path along its axis. Once this distance is minimized, the interstitial is trapped by the vacancy, but it cannot recombine until a longer time scale associated with the rotation barrier has passed. Assuming a prefactor of 10^{13}/s, this time will be about 5 ms at $T=300$ K. Thus, while oxygen defects will essentially trap one another, eliminating their mobility, they will not necessarily recombine. That this rotation mechanism has a much longer waiting time is confirmed by the collision cascade simulations of Ref. 14, which did not see recombination when the interstitial and vacancy were not aligned.

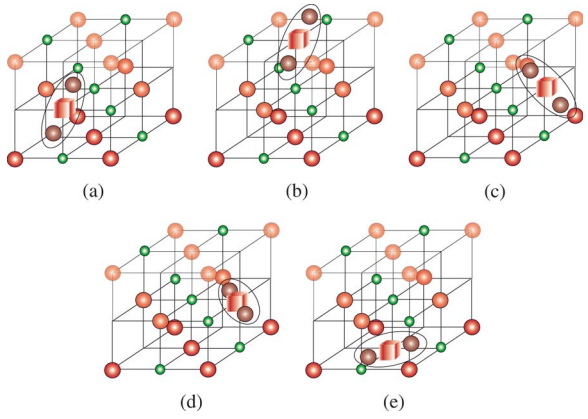

FIG. 2. (Color online) Diffusion of an oxygen split interstitial in $MgAl_2O_4$. The interstitial overcomes an activation energy of 0.29 eV to diffuse along its axis, as shown in (a) and (b). Reorientation mechanisms occur with barriers of 0.67 and 0.64 eV for transitions from configuration (b) to (c) and from (d) to (e), respectively. The cube represents a vacant oxygen site. Large dark spheres indicate the position of the interstitial oxygen ions.

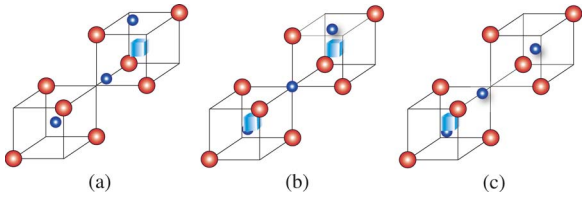

FIG. 3. (Color online) $Mg_i^{\cdot\cdot}$-V_{Mg}''-$Mg_i^{\cdot\cdot}$ split interstitial diffusion in spinel. The Mg split interstitial moves from (a) to (c) via the saddle shown in (b). The activation barrier for this process is 0.56 eV. The cube represents a Mg vacancy.

The structure of the Mg interstitial is also a split interstitial and also diffuses via an interstitialcy mechanism, as shown in Fig. 3. However, its diffusive nature is three dimensional, in contrast to the O interstitial. There are two Mg interstitial diffusion mechanisms, one with a barrier of 0.56 eV (which is the one illustrated in Fig. 3) and a second with a barrier of 0.74 eV. Thus, Mg interstitial diffusion is significantly slower than O interstitial diffusion. The lower energy saddle involves a rotation of the axis plus translation of the split interstitial while the higher energy saddle is a pure translation. This higher energy saddle would lead to one-dimensional diffusion, while the lower energy saddle allows for isotropic diffusion.

The isolated Al interstitial is unstable. It was never observed in the collision cascades[14] and, when a TAD simulation is performed beginning with an Al interstitial, it immediately relaxes to a split Mg-Al interstitial centered around a Mg lattice site. This structure itself is only metastable: with a barrier of 0.57 eV, it decays to a pure Mg split interstitial, as described above, and an $Al_{Mg}^{\cdot}$ antisite. As these two defects both have a net positive charge, they repel one another with the result that the Mg interstitial is free to migrate.

2. Vacancies

In a perfect spinel structure, each oxygen ion would have 12 nearest oxygen neighbors at equal distances. However, as illustrated in Fig. 4, because of the distortion of the oxygen sublattice mentioned above, the oxygen neighbors of any given oxygen ion separate into three classes: three oxygen neighbors at the closest distance of 2.47 Å (neighbors 4, 5, and 6), six at an intermediate distance of 2.89 Å (7–12), and three at the furthest distance of 3.27 Å (1, 2, and 3). If an oxygen vacancy is placed at the central site, then there are three different types of moves it can make. It can move to sites 4, 5, or 6 with a barrier of 1.49 eV. Motion to the intermediate range sites (7–12) has a larger barrier of 1.66 eV. Finally, we never observed a single event in the TAD simulations in which the vacancy moved to the furthest neighbors (1, 2, or 3). Using NEB, we find a barrier of 3.65 eV for this process. The oxygen vacancy moves by ex-

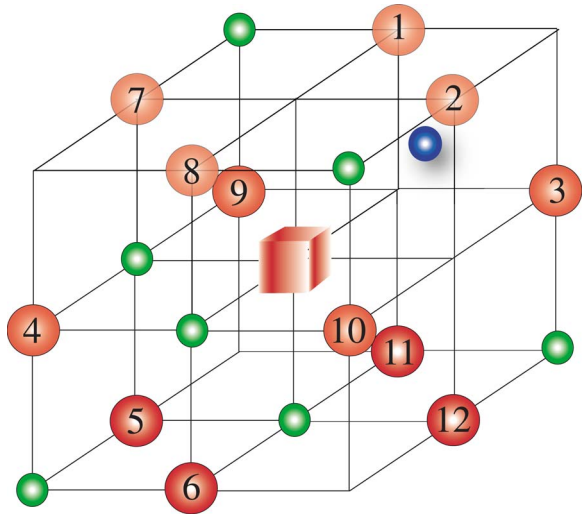

FIG. 4. (Color online) Part of the normal spinel structure containing an oxygen vacancy (red cube) is shown with its 12 first nearest neighbor anions. The distance between the central vacancy and ions 4, 5, and 6 is 2.47 Å, 2.89 Å for ions 7 -12 and 3.27 Å for the anions at 1, 2, and 3. The barriers for diffusion of the central vacancy to sites 4, 5, 6, and 7 -12 are 1.49 and 1.66 eV, respectively.

ecuting simple ⟨110⟩ moves on the oxygen sublattice. For net diffusion to occur, hops to the intermediate neighbors must occur; otherwise, the oxygen vacancy just hops between the four sites defining the nearest set of oxygen positions.

Cation vacancy diffusion is very similar for both types of cations. First, there is an intermediate state of split vacancy formation, where the displaced cation sits at an interstitial position midway between the two vacancies. For example, the V''_{Mg} results in the split vacancy V''_{Mg}-$Mg_i^{\cdot\cdot}$-V''_{Mg}, with the moving Mg ion occupying an octahedral site as illustrated in Fig. 5(c). The activation energy for this process is 0.68 eV. From this site, there is a small energy barrier of 0.09 eV for this ion to recombine with either vacancy. The barrier for Al vacancy migration is much higher, 2.00 eV, so that Al vacancies are practically immobile at 300 K.

While the Al vacancy is stable, and can diffuse as mentioned, it can transform to other species. With a barrier of 3.28 eV, it can convert into $Mg'_{Al}+V''_{Mg}$. As with the decay of the Al interstitial, these two defects have the same relative charge (negative here). They therefore repel and the Mg vacancy diffuses freely. This conversion is uphill in energy;

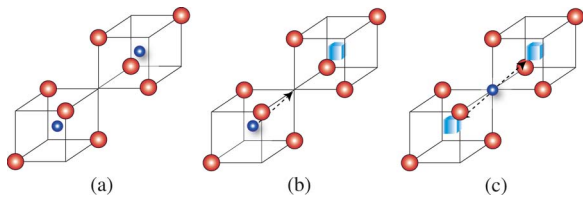

FIG. 5. (Color online) Mg vacancy diffusion in normal $MgAl_2O_4$ spinel. (a) The perfect lattice. The Mg vacancy (b) overcomes a barrier of 0.68 eV to form the split vacancy (c), where the interstitial occupies an octahedral site. The Mg interstitial in (c), can recombine to either of the two V''_{Mg} with a small barrier of 0.09 eV.

statics calculations find a value of 0.20 eV for the energy of the products, separated to infinity, relative to V'''_{Al}.[21]

To summarize point defect properties in $MgAl_2O_4$, the fastest diffusing species is the oxygen interstitial. It diffuses one dimensionally in a ⟨110⟩ direction with a barrier of 0.29 eV and has a barrier to reorient of about 0.64 eV. The Mg interstitial diffuses three dimensionally with a barrier of 0.56 eV while the Al interstitial is not stable and decays to an Al antisite and a Mg interstitial. Vacancy diffusion on both the oxygen and Al sublattices is much slower than for the corresponding interstitials. The Al vacancy diffuses with a barrier of 2.00 eV. It can convert into $Mg'_{Al}+V''_{Mg}$ with a barrier of 3.28 eV, though this process is uphill in energy. On the other hand, Mg vacancy migration is only slightly slower than Mg interstitial migration (the difference in migration energy is only about 0.1 eV)

B. Chemical composition effects: Diffusion in normal $MgGa_2O_4$ and $MgIn_2O_4$

Neither $MgGa_2O_4$ nor $MgIn_2O_4$ exist in nature in a normal, or $i=0$, state. Both have a relatively high level of inversion compared to $MgAl_2O_4$: for $MgGa_2O_4$, $i\sim0.5$ (Ref. 23) and for $MgIn_2O_4$, $i\sim1$.[24] However, to separate the role of chemical composition from that of disorder or inversion in point defect diffusion, we have examined point defect diffusion in normal versions of both spinels.

1. $MgGa_2O_4$

Table I summarizes our results on point defect diffusion in both $MgGa_2O_4$ and $MgIn_2O_4$. In $MgGa_2O_4$, the behavior of point defects is very similar to $MgAl_2O_4$. The oxygen interstitial again diffuses one-dimensionally, though with a slightly higher barrier of 0.47 eV. The barrier for rotation is also slightly higher at 0.79 eV. The barrier for oxygen vacancy migration is also higher than in $MgAl_2O_4$ at 2.02 eV. This is the barrier for diffusion to the second set of nearest oxygen neighbors, as required for net diffusion. The barrier for hops to nearest oxygen neighbors is 1.47 eV. Neglecting the effects of cation disorder, oxygen Frenkel pair recombination will be slower in $MgGa_2O_4$ compared to $MgAl_2O_4$.

As for cation diffusion in $MgGa_2O_4$, the Mg interstitial actually diffuses faster than in $MgAl_2O_4$ with a barrier of 0.48 eV. Mg vacancy migration is essentially the same as in $MgAl_2O_4$ with a diffusion barrier of 0.67 eV. Thus, relative to $MgAl_2O_4$, the rate of Mg Frenkel pair recombination will be somewhat faster, with the change being due to the faster diffusivity of the Mg interstitial.

Finally, as in $MgAl_2O_4$, the B cation interstitial, in this case Ga, is not stable and decays upon relaxation to $Ga_{Mg}^{\cdot}+Mg_i^{\cdot\cdot}$. The Ga vacancy can diffuse three dimensionally with a barrier of 1.82 eV, lower than the Al vacancy in $MgAl_2O_4$.

2. $MgIn_2O_4$

In contrast, point defect behavior in $MgIn_2O_4$ differs significantly from that in $MgAl_2O_4$ and $MgGa_2O_4$. The oxygen interstitial diffuses three-dimensionally. In its ground state, it again has a split interstitial structure just as in $MgAl_2O_4$ and $MgGa_2O_4$. However, by going over a barrier of 0.54 eV it

can access a metastable state at an energy of 0.39 eV. This metastable state is a pure interstitial structure which can move in one of several ⟨100⟩ directions with a barrier of 0.15 eV. These moves seem to be constrained to a subset of sites (similar to the low barrier event for the oxygen vacancy in $MgAl_2O_4$). However, from this structure, the interstitial can decay back to the split structure but with a different position and orientation. This decay also has a barrier of 0.15 eV. Thus, via these combination of moves, the oxygen interstitial in $MgIn_2O_4$ can diffuse three dimensionally with a net diffusion barrier of 0.54 eV.

The oxygen vacancy in $MgIn_2O_4$ has, in theory, three types of diffusive jumps, just as in $MgAl_2O_4$ and $MgGa_2O_4$. However, the barrier for the jump to the nearest oxygen neighbors is so fast (0.29 eV), that we have not observed the jump to the second nearest oxygen neighbors required for net diffusion in our TAD simulations. We have calculated this barrier with NEB, finding a value of 1.83 eV. This value is actually smaller than that in $MgGa_2O_4$, but because the first barrier is so much smaller, about 10^{26} of the fast events would occur for every one of the slow events at room temperature, explaining why it was not seen in the TAD simulation.

The trend from $MgAl_2O_4$ to $MgGa_2O_4$ continues to $MgIn_2O_4$ for the Mg interstitial migration barrier. It is fastest in $MgIn_2O_4$, with a barrier of 0.32 eV. The barrier for Mg vacancy migration is largest in $MgIn_2O_4$ with a value of 0.97 eV. However, we find that, in $MgIn_2O_4$, the Mg vacancy is only metastable and decays, with a barrier of 2.16 eV, to $In^{\cdot}_{Mg}+V'''_{In}$. This process is about 1.5 eV downhill in energy relative to the Mg vacancy. As these defects have opposite charge, they are bound to one another. Statics calculations reveal that the Mg vacancy in $MgAl_2O_4$ is also only metastable. However, the decay rate relative to the hopping rate must be slower in $MgAl_2O_4$, as we did not directly observe the decay in the TAD simulations on $MgAl_2O_4$. Statics calculations indicate the binding energy in that case is 1.72 eV, relative to separated $Al^{\cdot}_{Mg}+V'''_{Al}$.

Finally, as in the other two spinels, the B cation interstitial is not stable in $MgIn_2O_4$ and decays to a $In^{\cdot}_{Mg}$ antisite and a Mg interstitial which then is free to diffuse. The In vacancy diffuses much as the *B* cation vacancies in the other spinels but with a much lower diffusion barrier of 0.90 eV.

It is worth examining the trends in defect mobility as a function of the differences in the three spinels. There are two principle differences between the three spinels: the O-*B* interaction and the lattice constant. As discussed in Ref. 14, as *B* is changed from Al, to Ga, to In, the O-*B* interaction becomes stiffer. All things being equal, we would expect that motion of especially oxygen would be more difficult, then, in $MgIn_2O_4$ as compared to $MgAl_2O_4$. This is exactly what we observe for the oxygen interstitial. In the case of the Mg interstitial, all of the interactions of the moving atom, the Mg interstitial, are identical in all three spinels. The main difference is now the lattice constant, with $MgIn_2O_4$ having a larger lattice constant than $MgGa_2O_4$, which has a larger lattice constant than $MgAl_2O_4$. This would suggest that the Mg interstitial would move more easily in $MgIn_2O_4$ and again that is what we observe.

The situation for the vacancies is more complex as no clear trend is observed among the three spinels as a function of these differences. It is likely, therefore, that these differences start competing, with the stiffer potential dominating in some instances while the increased lattice constant is more important in others. In these cases, an explicit calculation is required in order to determine which aspects dominate and the actual value of the migration barrier.

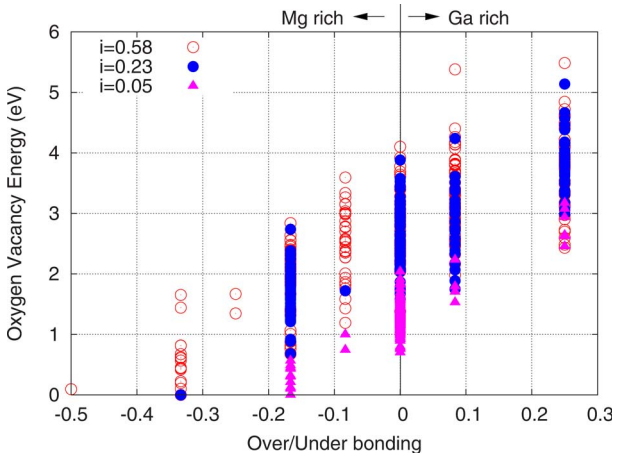

FIG. 6. (Color online) Energy of oxygen vacancy states versus over/under bonding values for $MgGa_2O_4$ as a function of inversion, relative to the lowest energy site. As the inversion is increased, more local environments become available. For the most inverted spinel (i=0.58), the energies of the different oxygen vacancy sites span an energy range of about 5.5 eV. There is a clear preference of the oxygen vacancy for sites that are underbonded or Mg rich.

In summary, the main differences between the three normal spinels occur for $MgIn_2O_4$, where oxygen interstitial diffusion is three dimensional instead of one dimensional as in $MgAl_2O_4$ and $MgGa_2O_4$ and the *B* cation vacancy diffuses significantly faster than in the other two spinels. This gives a sense of the chemical composition effects on point defect diffusion in these spinels. However, as mentioned, cation disorder is always present in spinels, to an especially high degree in $MgGa_2O_4$, and that also plays a role on defect diffusion, a role we investigate in the next section.

IV. DEFECT KINETICS IN DISORDERED SPINELS

A. Defects in disordered spinels

Unlike in normal spinels, where point defects diffuse via well-defined pathways through the structure, diffusion in disordered spinels is much more complex. Taking oxygen as an example, in normal spinel, each oxygen ion has an environment equivalent to all other oxygen ions. However, once disorder is introduced, the mixing of the *A* and *B* sublattices results in many different local environments for oxygen ions. Here, we examine the impact this has on diffusion.

Using the MC scheme mentioned above, we have generated cells of $MgGa_2O_4$ with various levels of inversion. Figure 6 shows how the local environment of oxygen impacts the energetics of the oxygen vacancy as a function of inversion. In Fig. 6, the local environment is measured via the over/under bonding of the oxygen site. This over/under bonding is defined by the number of electrons the cations

surrounding the oxygen site have to donate to that oxygen site. For example, each Ga ion has three electrons to donate to neighboring oxygen ions while the Mg ions have two electrons. Cations on tetrahedral sites (always Mg in normal spinel) share electrons with four oxygen neighbors while cations on octahedral sites share their electrons with six oxygen ions. In normal spinel, this leads to the cations donating $\frac{2}{4}+3\frac{3}{6}=2$ electrons to each oxygen ion, which is how many electrons the oxygen ion accepts in normal spinel. The difference between how many electrons are available for the oxygen ion and how many it requires (2) is the over/under bonding value plotted in Fig. 6. In normal spinel, this is always equal to zero.

In disordered spinel, different anions see different local cation arrangements and the over/under bonding is not zero for all sites. This is in fact what we observe in the disordered spinel, as shown in Fig. 6. Furthermore, we see a strong correlation between the over/under bonding and the energy of the oxygen vacancy. Roughly, as the local environment goes from Mg rich (negative over/under bonding) to Ga rich, the energy of the oxygen vacancy increases. Thus, oxygen vacancies strongly prefer Mg rich environments and the energy differences between sites span a range of about 5.5 eV in the most inverted spinel. These Mg rich environments will effectively act as traps for oxygen vacancies.

Oxygen interstitials, on the other hand, tend to favor Ga rich environments. However, the trends are not nearly as strong as in the case of the vacancy. We have not explored the oxygen interstitial as thoroughly as the oxygen vacancy just because the structure is more complex, with multiple possible arrangements of the split interstitial structure for each oxygen lattice site. We also see strong dependencies of cation defect energies as a function of local environment.

$MgIn_2O_4$ behaves very similarly to $MgGa_2O_4$. However, as $MgIn_2O_4$ is more ordered than $MgGa_2O_4$ (the tetrahedral sites are all occupied by In cations), the variations are not as great. For example, the energy of the oxygen vacancy as a function of environment only varies over a range of about 1.2 eV for $i=1$.

Thus, in contrast to normal spinel, disordered spinels have strongly preferred sites for different kinds of defects. This will both inhibit diffusion (oxygen vacancies will strongly prefer to reside in Mg rich sites, for example) as well as recombination, since oxygen vacancies and interstitials tend to prefer opposing environments. To verify these conclusions, we have performed TAD simulations in both half-inverse ($i=0.5$) $MgGa_2O_4$ and fully inverse ($i=1$) $MgIn_2O_4$. The cells used in these simulations were based on $2\times1\times1$ disordered cells.

In the discussion that follows, we have stopped indicating the charges on the defects in the Kröger-Vink notation. This is because the charge is meaningful only relative to some well defined state. The disordered state is not so well defined, so we feel it is not a good reference state. At the same time, the $i=0$ structure is also not a good reference, as at temperature ions do not prefer to sit on the corresponding $i=0$ sites. Thus, for clarity, we have decided to remove the charges from the defects in the discussion of disordered spinels.

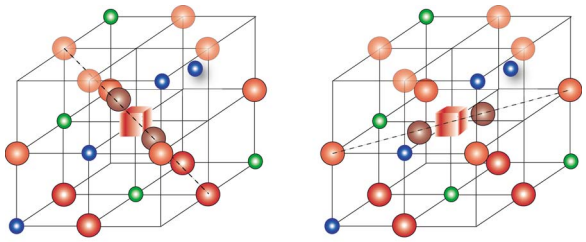

FIG. 7. (Color online) Rotation mechanism for the O_i-V_O-O_i split interstitial in the half-inverse $MgGa_2O_4$. The activation energy is 0.86 eV for the transition from configuration (a) to (b).

B. Defect kinetics in disordered spinels

TAD simulations confirm the view of defect diffusion in disordered spinels described above. While in normal spinels, defects diffuse throughout the simulation cell (though, in some cases, in a constrained manner), in disordered spinels, defects are typically confined to just a few sites and are unable to diffuse throughout the cell. In this section, we briefly describe the types of events seen in these simulations, to better understand how disorder affects the details of point defect kinetics.

For defects in both disordered $MgGa_2O_4$ and $MgIn_2O_4$, many more types of events occur in the system than in normal spinel. Many have analogs to what was observed in the normal spinels, but, because of the disorder, the same type of event has different barriers depending on the local environment of both the initial and final state. There are, in addition, new types of events that occur that were not observed in the normal spinels.

We have not explored what happens to a defect in all possible environments in these disordered spinels. Rather, we chose representative initial structures and followed the behavior of those defects out in time as far as was reasonable. It is possible that other behavior might occur for other local environments, but we believe these simulations are representative of what would occur for other conditions.

1. Half-inverse spinel, $MgGa_2O_4$

In half-inverse $MgGa_2O_4$, we observe that the oxygen interstitial still moves primarily in ⟨110⟩ directions, just as in normal spinel. It is also able to rotate to other orientations. However, a new type of event also occurs in which the rotation takes place around the central vacancy rather than via an interstitialcy mechanism. This new mechanism is illustrated in Fig. 7. The energy barrier for this particular rotation mechanism is 0.86 eV, though other realignment mechanisms were observed with barriers as low as 0.33 eV (compared to 0.79 eV in normal $MgGa_2O_4$ spinel).

The trend seen in the static calculations for the oxygen vacancy to strongly prefer Mg-rich areas is directly observed in the TAD simulations. When an oxygen vacancy is placed in a site with four Ga neighbors, it moves, via a sequence of events with barriers of 0.78, 0.59, and 0.85 eV, to find a site with one Ga and three Mg neighbors and is essentially trapped there for the duration of the simulation. This final

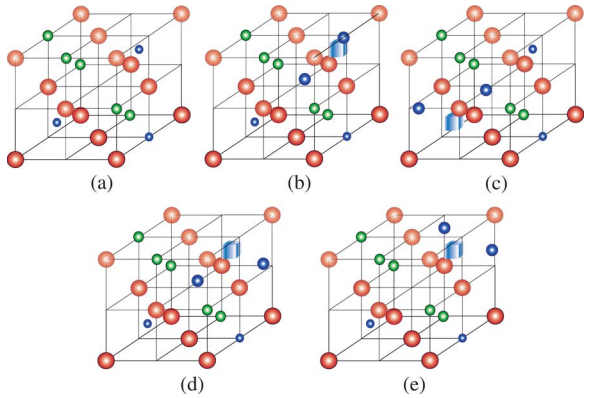

FIG. 8. (Color online) Diffusion of Mg split interstitial in the disordered $MgGa_2O_4$ spinel. (a) Perfect structure. (b) Mg_i-V_{Mg}-Mg_i aligned along ⟨110⟩ with both Mg_i filling octahedral sites. The central interstitial does not sit identically at the center of the cell because of the disorder in the cell. Three observed mechanisms are shown from configurations (b) to (c), (b) to (d), and (b) to (e) with corresponding barriers of 0.15, 0.09, and 0.56 eV, respectively.

state is 4.06 eV lower in energy than the initial state. Compare the barriers here to that in normal $MgGa_2O_4$ spinel for oxygen vacancy diffusion of 2.02 eV.

Only three distinct types of events were observed during one simulation of a Mg split interstitial in which 526 events were accepted. As illustrated in Fig. 8, one event, with a barrier of 0.15 eV, led to diffusion of the interstitial to a neighboring site while the other two, with barriers of 0.09 and 0.56 eV, resulted in the reorientation of the split interstitial structure to a new ⟨110⟩ orientation. Other simulations revealed translation mechanisms similar to that shown in Fig. 8(b) and 8(c), but with somewhat higher barriers of up to 0.60 eV. However, in no case was net diffusion through the cell observed.

The Mg vacancy, when placed on an octahedral site, is essentially trapped there. It undergoes local rearrangements by forming a split vacancy structure with a nearby tetrahedrally coordinated Mg ion, but always returns to the original structure. It is also able to convert into $Ga_{Mg}+V_{Ga}$ with a barrier of 2.02 eV, similar to what was seen for V_{Mg} in $MgAl_2O_4$. In contrast, in a simulation in which the Mg vacancy was initially placed on the tetrahedral site, it made several diffusive jumps via mechanisms similar to that shown in Fig. 5, until it induced the formation of a cation disorder defect pair $Ga_{Mg}+Mg_{Ga}$. This was accompanied by the Mg vacancy moving to an octahedral position. At that point, it was then trapped through the interaction with the disorder defects. The time scale for this to occur was 6.4 μs at $T=600$ K. The formation of cation disorder defects via point defects in the lattice suggests that inversion may be induced by non-stoichiometry, similar to the concepts proposed by Refs. 25 and 26.

Defects involving Ga, both interstitials and vacancies, were observed to be only metastable. Split interstitial structures Mg_i-V_{Mg}-Ga_i, Mg_i-V_{Ga}-Ga_i, and Ga_i-V_{Ga}-Ga_i decay fairly quickly to other defects. The first structure decays to $Ga_{Mg}+Mg_i$ after 1.5 ns at $T=300$ K, while, in a fraction of a picosecond at $T=300$ K, the second decays to Mg_i after the Ga ion recombines with the Ga vacancy. The third structure is not stable at all; upon minimization, it transforms to the first structure which again decays to $Ga_{Mg}+Mg_i$.

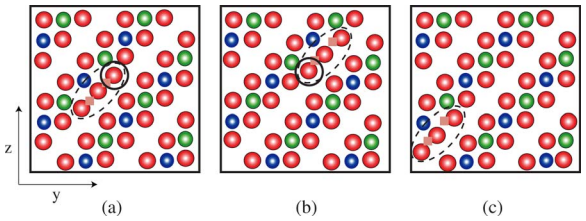

FIG. 9. (Color online) Diagram illustrating the 1D diffusion of the O_i-V_O-O_i-V_O-O_i crowdion in the $MgIn_2O_4$ crystal. The crowdion is identified by the dashed ellipse while the continuous circle denotes the O interstitial with four nearest In neighbors. $E_a=0.32$ eV for transition (a) to (b) but $E_a=0.89$ eV for transition (a) to (c).

Similarly, the Ga vacancy, whether on a tetrahedral or octahedral site, decays to $Mg_{Ga}+V_{Mg}$. Thus, Ga defects tend to decay, leading to mixing on the cation sublattice (local antisites) and Mg defects.

The main conclusion from the TAD simulations on the half-inverse spinel is that defect mobility is severely limited compared to normal spinels. While elementary motions are similar to those in the normal spinels, the defects are essentially trapped by the disorder in the half-inverse spinel and cannot easily diffuse through the cell, at least on the time scales accessible with TAD. Often, point defects induce cation mixing. This is especially true for Ga defects, which tend to decay to cation disorder defects and Mg point defects.

2. *Inverse spinel,* $MgIn_2O_4$

Defect behavior in inverse $MgIn_2O_4$ is similar to that in half-inverse $MgGa_2O_4$. The main difference is that, as observed in collision cascades,[14] interstitial defects tend to be more extended and form crowdions. This is illustrated in Fig. 9 for the oxygen interstitial. The split structure seen in normal spinels extends to form a crowdion that is represented by three interstitials and two vacancies in Fig. 9. One of the oxygen interstitials has four In nearest neighbors and, as discussed above, oxygen interstitials tend to prefer B^{3+}-rich environments. Thus, the crowdion is trapped at this location. It oscillates between two nearly equivalent positions with a barrier of 0.32 eV. It can "break free" to the configuration in Fig. 9(c) by overcoming a larger barrier of 0.89 eV, though it very quickly returns to the original location. It was also observed to rotate to other ⟨110⟩ orientations with barriers between 0.80 and 1.33 eV, but it never left the immediate vicinity of its starting location.

Oxygen vacancy behavior was characterized by the motion of the vacancy from In-rich environments to Mg-rich environments, just as in $MgGa_2O_4$. This diffusion occurred via barriers of between 0.60 and 1.36 eV, comparable to the barrier in normal $MgIn_2O_4$ spinel.

Crowdions, the structure of which is illustrated in Fig. 10, are also observed on the In sublattice. In the TAD simulation, the crowdion was observed to oscillate between two structures but, again, no net diffusion was seen. Simulations

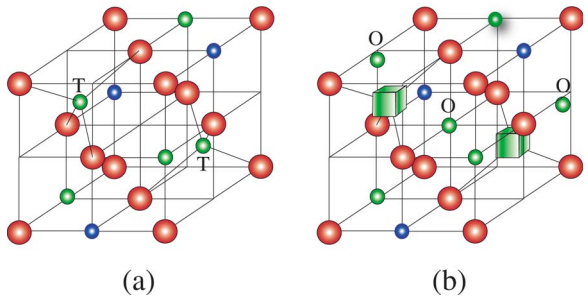

FIG. 10. (Color online) (a) Part of the inverse $MgIn_2O_4$ spinel with "T" denoting In ions with tetrahedral coordination. (b) Stable crowdion defect where an extra In interstitial displaces the tetrahedral ions to octahedral sites labeled "O." The cubes represent In vacancies.

of two other interstitial structures, In_i-V_{In}-Mg_i and Mg_i-V_{In}-Mg_i, while not forming crowdions, also exhibited no net diffusion.

In $MgIn_2O_4$, since it is fully inverse ($i=1$), all Mg ions reside on octahedral sites. The Mg vacancy stays on the Mg sublattice, executing hops with a barrier of about 1 eV. The octahedrally coordinated In vacancy decays to a Mg vacancy and Mg_{In}. The tetrahedrally coordinated In vacancy forms a split vacancy structure in which an In ion resides at an octahedral interstice midway between two tetrahedral vacancy. This structure is consistent with the In crowdion structure in that In ions tend to move into octahedral interstice sites. This is also seen in the collision cascades,[14] where In ions segregate to octahedral sites under irradiation. As in all cases in the disordered spinels, no net diffusion is observed for any of these defects.

As in $MgGa_2O_4$, we observe no net diffusion of point defects on the time scales accessible to TAD in $MgIn_2O_4$. It is clear, then, that the disorder greatly complicates and inhibits the motion of point defects through the spinel structure. However, we are unable to probe the defect kinetics sufficiently with TAD to understand the quantitative impact disorder has on diffusion in these materials. For that reason, we use kinetic Monte Carlo (KMC) to probe the very long-time behavior of one defect, the oxygen vacancy in $MgGa_2O_4$.

V. OXYGEN VACANCY DIFFUSION IN $MgGa_2O_4$

Even with the advantages offered by TAD, the time scales associated with net diffusion in the disordered spinels are still out of reach. We thus turn to KMC. The advantage of KMC is that it is significantly faster than even TAD for evolving a system forward in time. The disadvantage is that all possible events must be characterized in advance. For many systems, this is a nigh-impossible task. For the study here, we chose to study the oxygen vacancy in $MgGa_2O_4$ as it is a relatively simple defect. By this choice, however, we do not mean to imply that the oxygen vacancy is likely the most important defect for mass transport in these materials. We chose it solely for convenience.

We have generated $2\times2\times2$ cells with inversions of $i=0$, 0.05, 0.23, and 0.58. For cells with $i>0$, we have calculated, via NEB, the barrier for each of the 12 possible events for each vacancy site. We have also done this for the $2\times1\times1$ cell used to build the TAD simulation cell, which had an inversion of $i=0.5$. We then input these barriers into a KMC model in which we assumed the frequency prefactors for all events were 10^{13}/s. The resulting barriers are illustrated in Fig. 11 for the cases of $i=0.05$, 0.23, and 0.58, where they are plotted versus the energy difference between the final and initial state (ΔE_{fi}). For the smallest level of inversion, more states are clustered around $\Delta E_{fi}=0$ eV and there is less variation in both ΔE_{fi} and the saddle point energy. As the level of inversion is increased, more types of local environments are available (as also seen in Fig. 6) and the variation in ΔE_{fi} and the saddle point energy increases such that, by $i=0.58$, ΔE_{fi} spans a range of about 8 eV and the relative saddle point energies are as high as 6 eV. As one might expect, there is also a rough trend of the saddle point energy increasing with ΔE_{fi}. However, the trend is not so strong that a simple relation between the two quantities can be derived.

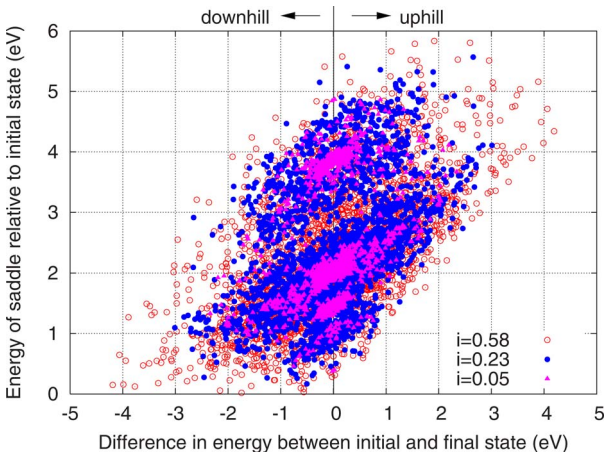

FIG. 11. (Color online) Barriers for oxygen vacancy motion in $MgGa_2O_4$ spinel with levels of inversion of $i=0.05$, 0.23, and 0.58. Saddle point energies are relative to the initial state they connect and they are plotted against the difference between the final and initial state energies.

It should be noted that the diffusion path of a defect will be specific to the particular random cell we use. Also, the periodicity of the cell used in these calculations is artificial. Future work will investigate which aspects of diffusion reported here are universal for a given level of inversion and which depend on the particular atomic arrangements.

Calculating the diffusivity for defects in disordered systems is not straightforward. Statistics becomes a real issue, especially at lower temperatures. We calculated the diffusivity in the normal way, by looking at the mean squared displacement (MSD) of the vacancy versus time:

$$\mathrm{MSD} = \frac{1}{N}\sum_{j=1}^{N} (\mathbf{r}_j - \mathbf{r}_{j-1})^2, \tag{3}$$

where each section of the trajectory j corresponds to a given length of time Δt. In order to ensure that our results were

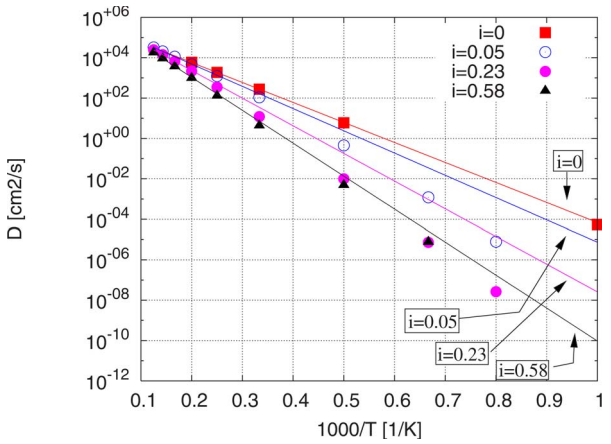

FIG. 12. (Color online) Diffusivity of the oxygen vacancy in $MgGa_2O_4$ spinel as a function of temperature and inversion i. The lines are fits to the high temperature results and represent the high temperature activation energy for diffusion for each level of inversion. At lower temperatures, the diffusivity deviates from the high temperature extrapolation.

converged, we increased Δt until the MSD attained a constant slope independent of Δt. For lower temperatures ($T=1000$ K or below), convergence required in excess of billions of KMC steps and we did not reach convergence in all of these cases. Thus, results for the lower temperatures are not reported.

Figure 12 shows the diffusivity of the oxygen vacancy as a function of temperature and inversion. The temperature range is much greater than experimentally achievable, as $MgGa_2O_4$ will definitely melt before such temperatures are reached [$MgGa_2O_4$ melts at about 2300 K (Ref. 27)]. However, the high temperatures provide a useful limit to the diffusion constant determined from the KMC simulations.

There are a number of points to notice from the figure. First, as expected from the properties of normal spinel (Table I), for $i=0$, the extracted activation energy is 2.0 eV. This is the barrier for the oxygen vacancy to move to the second nearest oxygen neighbor, which is required for net diffusion. This energy is also the limit for the activation energy for diffusion as i approaches 0.

Second, the activation energy increases with increasing inversion. The extracted high-temperature activation energies are 2.2 eV for $i=0.05$, 2.7 eV for $i=0.23$, and 3.2 eV for $i=0.58$. These activation energies are shown in Fig. 12 via the Arrhenius lines. As the inversion increases, the effectiveness of the traps, due to disorder, increases, slowing the migration of the oxygen vacancy. A fully disordered system is presumably a limit and, as the inversion increases further towards $i=1$, the diffusivity would be expected to increase again, approaching, but not reaching, the $i=0$ value.

Third, the diffusivity versus temperature is not linear, as would be expected from an Arrhenius process. As the temperature is decreased, the diffusivity decreases faster than is predicted by the high temperature Arrhenius behavior illustrated in Fig. 12. This is not altogether surprising, as studies on model disordered systems reveal diffusion to be non-Arrhenius in nature.[28] Indeed, it has been shown[29,30] that even a small amount of heterogeneity in a simple KMC model leads to non-Arrhenius diffusion. This is due to the fact that, because of the heterogeneous distribution of barriers, new pathways become activated as the temperature is increased. It has been observed that a distribution of site energies causes a downward curvature in the Arrhenius curve (the type of curvature we see in Fig. 12), while a corresponding distribution in saddle energies contributes to a postitive curvature. For a given distribution width, this effect is stronger for site energies than saddle energies, leading to a net negative curvature, as we observe here.[31]

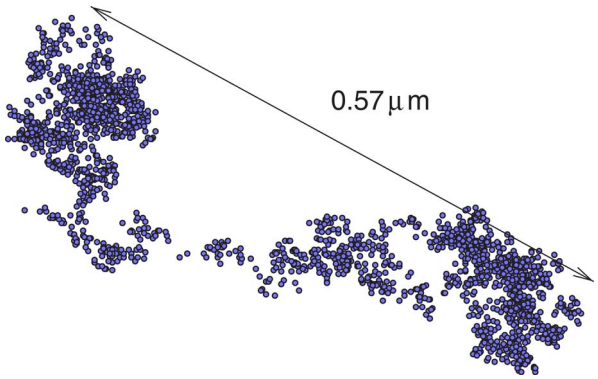

FIG. 13. (Color online) Trajectory taken by the oxygen vacancy in $MgGa_2O_4$ with $i=0.23$ and $T=2000$ K. The pseudo-one-dimensional nature of the path is evident. The trajectory becomes more isotropic with increasing temperature.

Finally, the amount of deviation in the diffusion constant at low temperatures, from the high-temperature Arrhenius behavior, is not consistent for different levels of inversion. The diffusivity falls off faster for $i=0.23$ than for $i=0.58$. This suggests that the details of diffusivity depend not just on the level of inversion i, but also on the details of the specific disordered structure. Future work will investigate this further.

As mentioned, we also performed simulations for the $2\times1\times1$ $i=0.5$ cell used in the TAD simulations. In that case, we found that the diffusion of the vacancy was not isotropic. In fact, it was essentially one dimensional, even at high temperatures, with preferred diffusion perpendicular to the long dimension of the cell. While it might be expected that locally diffusion could be anisotropic, over large enough distances in a real disordered spinel, diffusion should be isotropic. This is the reason we investigated the larger cell size of $2\times2\times2$. However, as illustrated in Fig. 13 for $i=0.23$ and $T=2000$ K, even there, the diffusion is not fully isotropic at low temperatures. There are definitely preferred directions for the vacancy to diffuse: the spatial extent of the trajectory in the x direction is three times as great as in y and four times as great as in z. Thus, even larger cells are necessary to accurately describe the long-range isotropic nature of these disordered spinels. In the simulation illustrated in Fig. 13, the vacancy migrated a distance of about 0.57 μm over a time of about 0.8 s.

Figure 14 shows the frequency with which events of a given barrier were accepted in the $i=0.23$ cell at $T=2000$ K. For a fully sampled system, the probability of crossing a given saddle will be proportional to the absolute saddle energy, independent of the energy of the minimum it

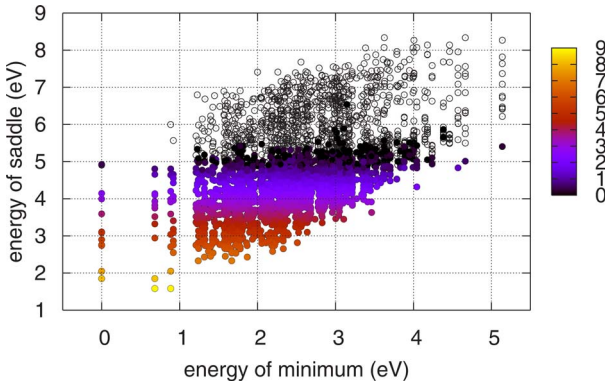

FIG. 14. (Color online) Events accepted in a KMC simulation of $MgGa_2O_4$ spinel with $i=0.23$ at $T=2000$ K. The color of the solid circles indicate how many times that event was accepted in the KMC simulation via the bar. The bar is a $\log_{10}$ scale, such that the events accepted the most were accepted 10^9 times. Open circles indicate events which were never accepted in the simulation.

passes through. The fact that the bands of constant acceptance number in Fig. 14 are parallel to the abcissa of the plot indicates that the space has been well sampled.

It is clear from these KMC simulations that disorder has a profound impact on the diffusivity of point defects. We intend to extend this study to include larger cells. We also need to accumulate statistics on the diffusivity for a given level of inversion, to understand how sensitively the values reported here depend on the detailed disordered structure. Another intriguing question is what happens when multiple defects are in the lattice. Even in a simple blocking model for multiple vacancies, in which a vacancy cannot move to a site already occupied by another vacancy, there will be a concentration dependence as some vacancies fill the trap sites, leaving other vacancies able to diffuse more quickly through the lattice.

VI. DISCUSSION AND CONCLUSIONS

We have examined point defect kinetics in spinels as a function of disorder using temperature accelerated dynamics (TAD) and kinetic Monte Carlo (KMC). We find that there are both chemical composition effects on defect kinetics as well as strong effects due to cation disorder. Point defect mobility tends to be fastest in $MgAl_2O_4$, as compared to normal $MgGa_2O_4$ and normal $MgIn_2O_4$, though there are exceptions, most notably the Mg interstitial, which diffuses fastest in $MgIn_2O_4$. The B cation interstitial (B=Al, Ga, or In) is unstable in all three normal spinels, decaying to an antisite plus a Mg interstitial.

Cation disorder greatly influences point defect mobility. Because of the disorder, each potential defect site has a different local environment and thus a different energy, leading to preferred sites for different types of defects. This preference is so great that, even with TAD, we are unable to probe sufficiently long times so as to observe net diffusion through the spinel. Using KMC to study the simplest possible defect, the oxygen vacancy, we find that the diffusivity of the defect is strongly dependent on the level of inversion. Furthermore, the diffusivity as a function of temperature is non-Arrhenius.

From the point of view of understanding the diffusion in disordered spinels, it would be ideal if the diffusivity depended on the level of inversion but not on the detailed structure of that inversion. At this point, it seems that at least some aspects of the diffusivity do indeed depend on the detailed structure. This seems to be true especially of the non-Arrhenius behavior in the diffusivity. However, it might be that the high-temperature diffusivity depends solely on the value of the inversion. While this might not be sufficient for explaining experimental observations, as this high-temperature range is beyond experimental conditions, it might still give some insight into how disorder impacts diffusivity in these materials. Future work will continue to examine this question.

Of the little previous work against which our results can be compared, most focuses on $MgAl_2O_4$. Upon irradiation with neutrons, $MgAl_2O_4$ exhibits very little swelling (see, e.g., Ref. 32). However, mechanical properties do change and this is interpreted as due to the formation of both cation and anion point defects.[32] Indeed, these changes in mechanical properties are reduced upon annealing, suggesting that point defect recombination is taking place.[32]

The most direct measurement of point defect migration was for irradiated $MgAl_2O_4$ in which dislocation loop size was monitored and a diffusion barrier for the rate-limiting vacancy was estimated.[33] While the identity of this vacancy could not be established, its migration barrier was found to be 2.0 ± 0.7 eV. This actually corresponds well to the value of 2.00 eV we obtain for V'''_{Al}. The barrier for V''_{Mg} is significantly lower (0.68 eV) while that of $V^{\cdot\cdot}_{O}$ is just slightly lower (1.67 eV) than the experimental value. This would suggest that V'''_{Al} is the rate controlling species for interstitial loop growth.

Oxygen self-diffusion has been measured in $MgAl_2O_4$ where a value of 4.55 ± 0.69 eV was obtained.[34] This value includes both the energy of formation as well as migration, so it is not so straight forward to compare to our results, as the formation energy depends on the specific reaction involved in creating the defect, which can be complicated in these complex oxides. The measured value is reduced somewhat in polycrystalline samples,[35] illustrating the importance of diffusion at grain boundaries.

Grimes[36] analyzed several experimental studies to extract formation and migration energies for ferritic spinels. In general, he found that oxygen vacancy migration energies were smaller than cation migration energies. While we find that B cation vacancies do diffuse slower than oxygen vacancies, Mg vacancies actually diffuse significantly faster. Grimes did not have enough data to extract formation and migration energies for $MgAl_2O_4$, but he does quote an overall activation energy for self-diffusion in $MgAl_2O_4$ of 3.74 eV from Lindner and Akerstrom.[37] Again, as this is a composite value, we are unable to directly compare it with our results.

It has been assumed in experimental analysis[38] that vacancy mobility is much smaller than interstitial mobility. We find this to be true for MgO,[39] in agreement with experimental estimates.[40] Experiments also find that vacancy mobility is much smaller than interstitial mobility in Al_2O_3.[40] However, in $MgAl_2O_4$, V''_{Mg} diffuses with a barrier (0.68 eV) very

similar to $Mg_i^{\cdot\cdot}$ (0.58 eV) and only somewhat larger than the fastest diffusing species O_i'' (0.29 eV). Thus, the assumption that vacancy mobility is always much smaller than interstitial mobility at low temperatures may be erroneous for spinels.

All of the results presented here are based upon an empirical potential which is a relatively simple description of these materials. However, in past work,[39,41,42] when we have compared the results from this potential with density functional theory, the trends in various properties (e.g., migration barrier vs interstitial cluster size, lattice parameter vs inversion) have been in qualitative agreement. We thus trust this potential to reveal the basic underlying physics of defects, if it does not attain quantitative accuracy. Furthermore, we have confirmed that the structures predicted by this potential for the various interstitial defects agree with density functional theory calculations. We will report on this in a future publication.[21]

That said, this potential does have limitations in how it describes the charges on ions. Ions always have a full formal charge in this model and charge transfer might be important in some cases, especially with regard to defects or during migration. Our past work[39,42] has shown that charge transfer is not so great for oxides such as MgO. However, it has been pointed out by a number of authors (e.g., Refs. 43 and 44) that ionization of defects can significantly alter their mobility. At this time, we are unable to fully explore the role of charge transfer in the processes described here. Even so, we expect that our results reveal qualitative trends in defect mobility that are representative of the real material.

We have been unable to find any previous work reporting on defect mobility or self-diffusion in either $MgGa_2O_4$ or $MgIn_2O_4$. Thus, it is not possible to verify our results on diffusivity as a function of inversion. It would be very interesting to perform experiments in which inversion was induced, possibly via irradiation, and diffusion measured as a function of that inversion. There would be many complications that would need to be accounted for, such as the annealing of radiation damage defects.

In MgO,[45] we found that interstitial defects form clusters that then behave as unique objects, exhibiting, in some cases, very high mobility. In spinel, while defects do tend to cluster, especially if they are of opposite charge, they do not form clusters which then exhibit mobility. Often, they form aggregates in which one ion may move quickly between two positions, but the center-of-mass of the cluster does not move on the time scales accessible with TAD. This suggests that any clustering will act as the nucleus of an extended defect such as an interstitial loop, trapping interstitials and leaving a vacancy bias.

In contrast to MgO,[39,45] as discussed above, oxygen vacancies and interstitials do not necessarily annihilate immediately, even when nearby. This is because the oxygen interstitial has an orientation and can only diffuse in certain directions. If that direction is not aligned with the nearby vacancy, there is a longer waiting time for the interstitial to rotate and then recombine. However, this does not necessarily result in defect accumulation. The two defects are still trapped by one another. This prevents the interstitial from diffusing away to a defect sink and leaving behind an unpaired vacancy. Eventually, the trapped interstitial will rotate and recombine, leading to recombination of the defect pair.

We have attempted to anneal the damage produced in collision cascades in $MgAl_2O_4$.[14] We are currently unable to anneal the full cascade with TAD, but we were able to anneal portions of several cascades. We find that, typically, the damage produced in $MgAl_2O_4$ reduces to a few antisite defects, if it does not anneal completely, on the time scales of 1 ns to 1 μs at $T=300$ K. This is consistent with the tendency of some point defects to decay to antisite complexes, as discussed above.

We have not used TAD to anneal the damage produced in collision cascades in the disordered spinels, as the traps created by the disorder prevent such simulations from being efficient. However, we have performed MD at an elevated temperature of 600 K to anneal damage from all three spinels. As the defects produced in the disordered spinels tend to be more concentrated than in the normal spinel, there is more immediate annealing in the disordered spinels. Interstitials and vacancies annihilate, creating either perfect material or cation disorder defects. However, this does not give much insight into the long time behavior of damage annealing as that will necessarily be governed by thermal events that are active on longer time scales than accessible via MD. While we are currently unable to directly probe this behavior for defects created during irradiation, our results here suggest that annhilation will be suppressed because of both the trapping of defects by the local environment as well as the segregation of interstitials and vacancies to opposing local environments.

That the diffusivity of these disordered spinels is greatly reduced from the normal value suggests some intriguing applications of these materials. In particular, they may make good diffusion barriers. In a number of technologies, including high-temperature superconducting tapes,[46] layers of material are deposited solely to reduce the diffusion of impurities into a key region of the substrate. Materials, such as $MgGa_2O_4$, which naturally accommodate a large amount of disorder may be ideal for this type of application.

This work was originally motivated by the problem of radiation tolerance in complex ceramics such as spinels. Past work has shown that the ability to accommodate disorder is a key indicator of a material's radiation tolerance.[47,48] However, disorder also leads to reduced diffusivity. At first glance, it seems reasonable that reduced defect mobility would be detrimental from a radiation recovery point of view as defect recombination will be inhibited. On the other hand, reduced mobility of point defects will necessarily suppress the nucleation and growth of extended defects, which leads to enhanced radiation tolerance (through reduced swelling). These effects are at crossed purposes and we do not know which, in fact, will dominate to determine damage evolution under kinetically controlled conditions. In addition, because of the disorder, different defect types tend to segregate to different (either Mg-rich or Ga-rich) regions in the material, further reducing the possibility of aggregation. Further work is needed to understand the impact that disorder has on radiation tolerance.

Finally, spinels might exhibit interesting percolation effects under irradiation. In normal ($i=0$) spinel, diffusion is relatively fast. If a normal spinel is subjected to irradiation,

regions of disorder will begin to form. In these disordered regions, created by the radiation-induced mixing of cations, diffusion will be retarded. As long as regions of normal spinel are connected, diffusing species will have access to the faster diffusion pathway throughout the spinel. However, once sufficient damage has been created so that the normal regions are no longer connected, diffusing species have no alternative other than to diffuse through disordered regions of the material, reducing their overall diffusivity. Thus, there will be a percolation transition, as a function of dose, beyond which diffusivity is reduced. Similar but opposite effects have been observed in irradiated material in which the irradiation process creates amorphous regions where diffusion is enhanced.[49]

To conclude, disorder introduces significant complexity into the kinetics of point defects. Thus, one must move past simple models of point defects and use higher level models to both understand point defect mobility over long time and length scales as well as characterize that mobility for continuum models and comparisons against experiment. The implications of the inhibited defect mobility on phenomena such as radiation damage is still not entirely clear.

ACKNOWLEDGMENTS

We thank P. Arendt, I. Usov, C. Stanek, and S. Murphy for useful discussions. This work was supported by the United States Department of Energy, Office of Science, Office of Basic Energy Sciences, Division of Materials Science and Technology. Los Alamos National Laboratory is operated by Los Alamos National Security, LLC, for the National Nuclear Security Administration of the U.S. Department of Energy under Contract No. DE-AC52-06NA25396.

[1] H. Matzke, V. V. Rondinella, and T. Wiss, J. Nucl. Mater. **274**, 47 (1999).
[2] T. Wiss and H. Matzke, Radiat. Meas. **31**, 507 (1999).
[3] F. W. Clinard, J. Nucl. Mater. **85-86**, 393 (1979).
[4] F. W. Clinard, G. F. Hurley, and R. W. Klaffky, Res. Mech. **8**, 207 (1983).
[5] F. W. Clinard, Ceram. Int. **13**, 69 (1987).
[6] K. E. Sickafus, A. C. Larson, N. Yu, M. Nastasi, G. W. Hollenberg, F. A. Garner, and R. C. Bradt, J. Nucl. Mater. **219**, 128 (1995).
[7] N. Bordes, L. M. Wang, R. C. Ewing, and K. E. Sickafus, J. Mater. Res. **10**, 981 (1995).
[8] M. Ishimaru, I. V. Afanasyev-Charkin, and K. E. Sickafus, Appl. Phys. Lett. **76**, 2556 (2000).
[9] S. J. Zinkle, H. Matzke, and V. A. Skuratov, in *Microstructural Processes in Irradiated Materials*, edited S. J. Zinkle *et al.*, MRS Symp. Proc. No. 540 (Material Research Society, Pittsburgh, 1999), p. 299.
[10] T. Wiss, H. Matzke, V. V. Rondinella, T. Sonoda, W. Assmann, M. Toulemonde, and C. Trautmann, Prog. Nucl. Energy **38**, 281 (2001).
[11] N. Yu, K. E. Sickafus, and M. Nastasi, Philos. Mag. Lett. **70**, 235 (1994).
[12] R. Smith, D. Bacorisen, B. P. Uberuaga, K. E. Sickafus, J. A. Ball, and R. W. Grimes, J. Phys.: Condens. Matter **17**, 875 (2005).
[13] D. Bacorisen, R. Smith, J. A. Ball, R. W. Grimes, B. P. Uberuaga, K. E. Sickafus, and W. T. Rankin, Nucl. Instrum. Methods Phys. Res. B **250**, 36 (2006).
[14] D. Bacorisen, Roger Smith, B. P. Uberuaga, K. E. Sickafus, J. A. Ball, and R. W. Grimes, Phys. Rev. B **74**, 214105 (2006).
[15] A. F. Voter, F. Montalenti, and T. C. Germann, Blood **32**, 321 (2002).
[16] A. F. Voter, in *Radiation Effects in Solids*, edited by K. E. Sickafus, E. A. Kotomin, and B. P. Uberuaga (Springer, NATO Publishing Unit, Dordrecht, The Netherlands, 2006), pp. 1–24.
[17] K. E. Sickafus, J. M. Wills, and N. W. Grimes, J. Am. Ceram. Soc. **82**, 3279 (1999).
[18] M. O. Zacate and R. W. Grimes, Philos. Mag. A **80**, 797 (2000).
[19] M. R. Sørensen and A. F. Voter, J. Chem. Phys. **112**, 9599 (2000).
[20] G. Henkelman, B. P. Uberuaga, and H. Jónsson, J. Chem. Phys. **113**, 9901 (2000).
[21] J. A. Ball, S. T. Murphy, R. W. Grimes, D. Bacorisen, R. Smith, B. P. Uberuaga, and K. E. Sickafus, Solid State Sci. (to be published).
[22] F. A. Kröger and H. A. Vink, *Solid State Physics: Advances in Research and Applications* (Academic, New York, 1957).
[23] J. E. Weidenborner, N. R. Stemple, and Y. Okaya, Acta Crystallogr. **20**, 761 (1966).
[24] J. B. Goodenough and A. L. Loeb, Phys. Rev. **98**, 391 (1955).
[25] A. Ibarra, R. Vila, and M. Jimenez de Castro, Philos. Mag. Lett. **64**, 45 (1991).
[26] R. I. Sheldon, T. Hartmann, K. E. Sickafus, A. Ibarra, B. L. Scott, D. N. Argyriou, A. C. Larson, and R. B. Von Dreele, J. Am. Ceram. Soc. **82**, 3293 (1999).
[27] C. W. W. Hoffman and J. J. Brown, J. Inorg. Nucl. Chem. **30**, 63 (1968).
[28] S. Havlin and D. Ben-Avraham, Adv. Phys. **51**, 187 (2002).
[29] C. H. Mak, H. C. Andersen, and S. M. George, J. Chem. Phys. **88**, 4052 (1988).
[30] D. S. Sholl, Langmuir **22**, 3707 (2006).
[31] J. Mössinger, A. Hörner, and H. Kronmüller, Phys. Status Solidi A **166**, 513 (1998).
[32] T. Yano, J. Am. Ceram. Soc. **82**, 3355 (1999).
[33] K. Yasuda, C. Kinoshita, K. Fukuda, and F. A. Garner, J. Nucl. Mater. **283-287**, 937 (2000).
[34] K. Ando and Y. Oishi, J. Chem. Phys. **61**, 625 (1974).
[35] Y. Oishi and K. Ando, J. Chem. Phys. **63**, 376 (1975).
[36] N. W. Grimes, Philos. Mag. **25**, 67 (1972).
[37] R. Lindner and A. Akerstrom, Z. Phys. Chem., Neue Folge **18**, 303 (1958).
[38] N. Bordes, K. E. Sickafus, E. A. Cooper, and R. C. Ewing, J. Nucl. Mater. **225**, 318 (1995).
[39] B. P. Uberuaga, R. Smith, A. R. Cleave, G. Henkelman, R. W. Grimes, A. F. Voter, and K. E. Sickafus, Phys. Rev. B **71**, 104102 (2005).

[40] S. J. Zinkle and C. Kinoshita, J. Nucl. Mater. **251**, 200 (1997).
[41] J. A. Ball, M. Pirzada, R. W. Grimes, M. O. Zacate, D. W. Price, and B. P. Uberuaga, J. Phys.: Condens. Matter **17**, 7621 (2005).
[42] G. Henkelman, B. P. Uberuaga, D. J. Harris, J. H. Harding, and N. L. Allan, Phys. Rev. B **72**, 115437 (2005).
[43] R. Devanathan, N. Yu, K. E. Sickafus, and M. Nastasi, Nucl. Instrum. Methods Phys. Res. B **127/128**, 608 (1997).
[44] C. Kinoshita, H. Abe, S. Maeda, and K. Fukumoto, J. Nucl. Mater. **219**, 152 (1995).
[45] B. P. Uberuaga, R. Smith, A. R. Cleave, F. Montalenti, G. Henkelman, R. W. Grimes, A. F. Voter, and K. E. Sickafus, Phys. Rev. Lett. **92**, 115505 (2004).
[46] P. N. Arendt and S. R. Folytn, MRS Bull. **29**, 543 (2004).
[47] K. E. Sickafus, L. Minervini, R. W. Grimes, J. A. Valdez, M. Ishimaru, F. Li, K. J. McClellan, and T. Hartmann, Science **289**, 748 (2000).
[48] K. E. Sickafus, J. A. Valdez, A. Cleave, M. Tang, M. Ishimaru, S. M. Corish, R. W. Grimes, C. R. Stanek, and B. P. Uberuaga, Nat. Mater. (to be published).
[49] K. Trachenko, M. T. Dove, T. Geisler, I. Todorov, and B. Smith, J. Phys.: Condens. Matter **16**, S2623 (2004).